JACS
JOURNAL OF THE AMERICAN CHEMICAL SOCIETY
Communication
pubs.acs.org/JACS

Diketopyrrolopyrrole-Containing Quinoidal Small Molecules for High-Performance, Air-Stable, and Solution-Processable n-Channel Organic Field-Effect Transistors

Yali Qiao, Yunlong Guo, Chunmeng Yu, Fengjiao Zhang, Wei Xu,* Yunqi Liu,* and Daoben Zhu*

Beijing National Laboratory for Molecular Sciences, Organic Solids Laboratory, Institute of Chemistry, Chinese Academy of Sciences, Beijing 100190, P.R. China

Supporting Information

ABSTRACT: We report the synthesis, characterization, and application of a novel series of diketopyrrolopyrrole (DPP)-containing quinoidal small molecules as highly efficient n-type organic semiconductors in thin film transistors (TFTs). The first two representatives of these species exhibit maximum electron mobility up to 0.55 cm^2 V^{-1} s^{-1} with current on/current off (I_{on}/I_{off}) values of 10^6 for **1** by vapor evaporation, and 0.35 cm^2 V^{-1} s^{-1} with I_{on}/I_{off} values of 10^5−10^6 for **2** by solution process in air, which is the first demonstration of DPP-based small molecules offering only electron transport characteristics in TFT devices. The results indicate that incorporation of a DPP moiety to construct quinoidal architecture is an effective approach to enhance the charge-transport capability.

Organic field-effect transistors (OFETs) have garnered much attention[1] in recent decades owing to their potential application in numerous electronic devices, such as radio frequency identification (RFID) tags, smart cards,[2] electronic papers, displays,[3] and sensors.[4] Presently, great progress in organic semiconductors (OSCs) has been made; however, the overall development of n-type OSCs still lags behind their p-type counterparts, especially in terms of performance, ambient stability, and so on.[5] Considering n-type OSCs playing significant roles in organic p−n junctions, bipolar transistors, and complementary logic circuits,[6] development of novel n-type semiconducting materials, particularly offering high performance, ambient stability, and solution processability, is a critical focus in organic electronics.[7]

Dicyanomethylene-substituted[8] quinoidal oligothiophenes, known as excellent electron acceptors and usually offering low-lying lowest unoccupied molecular orbital (LUMO) energy levels, have been extensively studied as n-type OSCs for application in OFETs, and some of them manifested very promising device performance. Frisbie et al.[9] reported that the electron mobility of butyl-modified quinoidal terthiophene was as high as 0.2 cm^2 V^{-1} s^{-1} under vacuum (thermal evaporated films at 130 °C). Takimiya et al.[10] designed a bis(hexyloxymethyl)cyclopentane-modified quinoidal terthiophene; the highest electron mobility reached 0.16 cm^2 V^{-1} s^{-1} under ambient atmosphere by solution process (after thermal annealing at 150 °C). To date, these performances are the best results for dicyanomethylene-substituted oligothiophene-based quinoids. Recently, Takimiya et al.[11] reported that ((alkyloxy)carbonyl)cyanomethylene and (acyl)-cyanomethylene, instead of the conventional dicyanomethylene group, are both effective terminal groups to construct new solution-processable n-type thienoquinoidals with good air stability.

Recently, diketopyrrolopyrrole (DPP)-based materials have being attracting much interest for their promising performance as a subunit for OSCs in OFETs,[12] organic photovoltaics (OPV)[13] and organic light-emitting diodes (OLEDs).[14] In terms of materials for OFETs, some DPP-based polymers afforded hole or ambipolar transport behavior with mobilities on the range of 0.1−1 cm^2 V^{-1} s^{-1}.[15] In addition, some DPP-based soluble small molecules manifested hole or ambipolar behavior with mobility on the order of 10^{-2} cm^2 V^{-1} s^{-1}.[16] However, DPP-containing materials with only electron-transport behavior have not been observed previously. Here, we directly modify the π-conjugated quinoidal core and report on the first two representative DPP-containing quinoidal small molecules **1** and **2** (Figure 1a, **1** and **2** with R = 2-ethyl-hexyl and 2-hexyl-decyl, respectively). The inclusion of a DPP moiety to the quinoidal architecture plays several important roles: (1) as a fused planar aromatic skeleton to enhance the π−π stacking and hence induce molecular ordering to increase charge-transport capability, (2) as an electron-deficient core to ensure a sufficiently low LUMO energy level to meet the requirement for air stability of n-type organic semiconductors, and (3) as a solubilizing group (alkyl groups on lactam N-atoms) to improve solubility for realization of solution-processability. Vapor-processed FETs based on **1** exhibit maximum electron mobility up to 0.55 cm^2 V^{-1} s^{-1} and solution-processed devices using **2** show that, at up to 0.35 cm^2 V^{-1} s^{-1} under ambient atmosphere, these electron mobilities are among the highest values reported for ambient-stable, especially solution-processed n-type OFET devices, suggesting that these DPP-containing quinoidal small molecules are promising candidates for n-type organic semiconductors.

Compounds **1** and **2** were synthesized from dibromo-substituted precursors **3** and **4**, respectively, using malononitrile and sodium hydride through a Pd-catalyzed Takahashi coupling reaction,[17] followed by oxidation with Br_2 in moderate yields (Figure 1a, see Supporting Information [SI] for details). The

Received: January 11, 2012
Published: February 21, 2012

dx.doi.org/10.1021/ja3003183 | J. Am. Chem. Soc. 2012, 134, 4084−4087

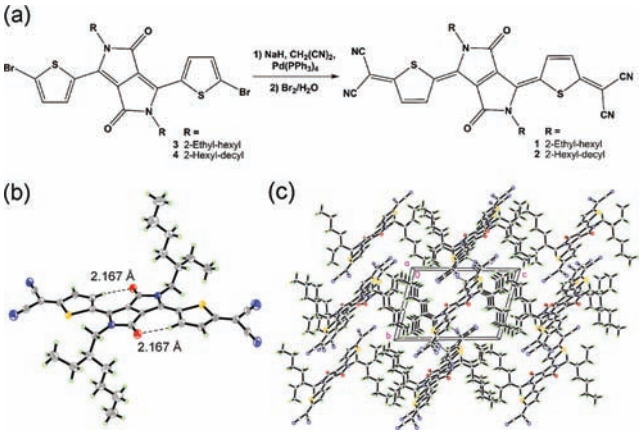

Figure 1. (a) Synthesis of compounds **1** and **2**. Single-crystal X-ray structure of compound **1**. (b) Molecular structure with 50% probability ellipsoids (C−H···O, 2.167 Å). (c) *a*-Axis projection representing a lamella-like packing (the solvent $CHCl_3$ is omitted for clarity).

solubility of **2** is quite high as expected (>10 mg mL^{-1} in $CHCl_3$ at rt), however, **1** with shorter branched alkyl chains is much less soluble (<3 mg mL^{-1}). Thermogravimetric analysis (TGA) shows that the thermolysis onset temperatures for **1** and **2** are 288 and 302 °C, respectively. In addition, differential scanning calorimetry (DSC) analysis displays that, for **2**, an obvious melting point was observed at 206 °C, and for **1**, no melting point could be observed before decomposition temperature (Figures S1−S4). The TGA and DSC results therefore reveal that **1** and **2** exhibit impressive thermal stability, enabling research on thin film crystallinity and microstructure over a broad range of temperature (from rt up to 200 °C).

Cyclic voltammograms of **1** and **2** in CH_2Cl_2 solution (Figure S5, Table S1) exhibit similar redox behavior, with two reversible reduction couples and no oxidation process observed (−1.2 to +1.6 V vs Ag/AgCl). The LUMO energy levels of **1** and **2** estimated from the first half-wave reduction potential (0.046 for **1** and 0.043 V for **2**) are both at approximately 4.51 eV below the vacuum level, well within the requirement for air-stable n-type OFET materials.[18] The absorption spectra of **1** and **2** (Figure S6) show almost identical strong absorption in the visible range, indicating that variation of the alkyl groups on the nitrogen atom in DPP moiety has almost no effect on the electronic structures for this series of quinoidal derivatives. The optical energy gaps (E_g), estimated from the onset of absorption, are 1.73 for **1** and 1.72 eV for **2**. The spectra of thin films (Figure S7) feature a bathochromic shift and broadening compared to the corresponding solution spectra. Moreover, shoulder absorption peaks appear for both compounds, which are at 723 nm for **1** and 721 nm for **2**. For the oligothiophene-based quinoidal derivatives, the phenomenon of simultaneous appearances of both small red shift and obvious shoulder absorption in thin film, especially at rt, has not yet been reported,[10,11] revealing that strong intermolecular interaction via the formation of π-stacking and/or J-type molecular aggregation[19] could be realized without any further thermal treatment of the thin films based on **1** and **2**.

Single crystals of **1** were obtained by slow evaporation of solvent from a dilute $CHCl_3$ solution (X-ray crystallographic data, see Table S2). The molecular structure (see Figure 1b) presents high planarity. Except for the branched alkyl substituent, the π-conjugated quinoidal backbone, including the cyano functional groups, assumes a significantly planar configuration with very small interplanar twist angles (Figure S8). Additionally, the intramolecular H bonds (C−H···O, 2.167 Å) lead to a cis conformation of the double bond linking the thiophene ring and DPP unit. As shown in Figure 1c, a lamella-like layered packing structure is observed, characteristic of the interdigitation of the branched alkyl substituent on the lactam N atoms of DPP. A columnar π-stacking structure ($\pi-\pi$ distance, 3.395 Å) along the long molecular axis direction is observed in a slipped face-to-face arrangement with a relatively large slippage of molecules (Figures S9−S11). In addition, a side-by-side H-bond interaction (C−H···N, 2.460 Å) between the β hydrogen of the thiophene ring and the nitrogen on the end-capped dicyanomethylenes is observed (Figure S12) that leads to the formation of a linear ribbon structure. The intramolecular nonbonded contacts, strong $\pi-\pi$ stacking, and side-by-side H-bond intermolecular interactions are significant for efficient charge-transport in OSCs.

OFET devices were fabricated with a top-contact device configuration on octadecyltrichlorosilane (OTS)-modified SiO_2 (300 nm)/Si substrate. Gold (Au) was used as drain and source electrodes. The drain−source channel length (L) is 0.08 mm and width (W) is 8.80 mm. All the FET measurements were performed under ambient atmosphere. The OFET results are summarized in Table 1, and typical characteristic curves are depicted in Figure 2. Devices based on **1** and **2** exhibited typical n-type semiconducting characteristics. For **1**, the FET performance of those devices was optimized by the variation of both substrate temperature and deposition speed (for details for device fabrication see SI). The maximum electron mobility is up to 0.34 $cm^2\ V^{-1}\ s^{-1}$ for **1** with normal deposition rate (rate increased from 0.5 to 10 Å min^{-1} for the first 10 nm and then maintained 10 Å min^{-1} for the last 20 nm, see SI for details) at 100 °C, while reaching 0.55 $cm^2\ V^{-1}\ s^{-1}$ with two-step deposition rate[20a] (the rate variation for the first 10 nm was the same as that for normal rate; then it continuously increased from 10 Å min^{-1} up to 3−6 Å s^{-1} for the last 20 nm) at 120 °C. As for **2**, solution-processed devices were successfully

Table 1. Maximum Electron Mobilities (μ_e[a]), Current On/Off Ratios (I_{on}/I_{off}), and Threshold Voltages (V_T) for OFET Devices Based on 1 and 2 on OTS-Modified Si/SiO_2 Substrate

	T (°C)	μ_e ($cm^2\ V^{-1}\ s^{-1}$)	I_{on}/I_{off}	V_T (V)
1	rt	0.20 (0.16 ± 0.04)[b]	10^6	12.2
	80	0.29 (0.24 ± 0.05)[b]	10^6	11.9
	100	0.34 (0.30 ± 0.04)[b]	10^6	11.5
		0.45 (0.40 ± 0.05)[c]	10^6	9.9
	120	0.07 (0.03 ± 0.04)[b]	10^6	11.2
		0.55 (0.50 ± 0.05)[c]	10^6	9.5
	150	—[b]	—	—
		0.01 (0.006 ± 0.004)[c]	10^4	11.7
2	rt	0.12 (0.09 ± 0.03)	10^4	6.2
	90	0.18 (0.15 ± 0.03)	10^4	7.7
	120	0.35 (0.29 ± 0.06)	10^5−10^6	−1.2
	150	0.01 (0.006 ± 0.004)	10^3	−19.6

[a]Average μ_e from about 10 devices with standard deviation. [b]Thin films were deposited with normal rate. [c]Thin films were deposited with faster rate.

dx.doi.org/10.1021/ja3003183 | J. Am. Chem. Soc. 2012, 134, 4084−4087

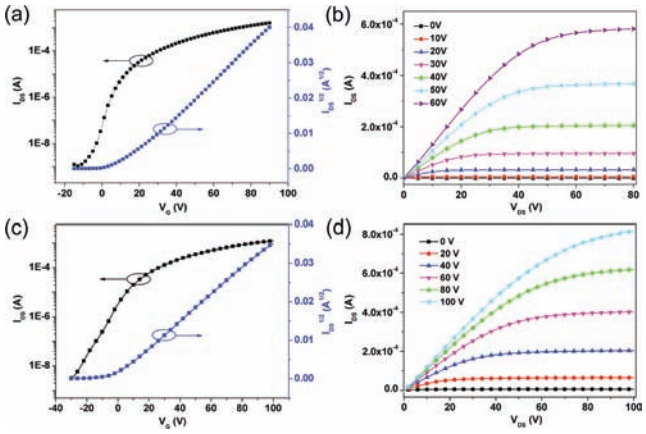

Figure 2. OFET characteristics for devices of compound **1** and **2** on OTS-modified SiO_2/Si after thermal treatment at 120 °C: (a) transfer curves at a constant source−drain voltage of 60 and 100 V for **1** and **2**, respectively; (b) output curves at different gate voltages.

fabricated, and the charge-transport performance was optimized by thermal annealing with maximum electron mobility up to 0.35 $cm^2\ V^{-1}\ s^{-1}$ and the I_{on}/I_{off} ratio up to 10^5−10^6, which is a promising candidate for practical application. Further, the thin films were characterized by atomic force microscopy (AFM) and X-ray diffraction (XRD) to understand the relationships between molecular structure, film morphology/crystallinity, and device performance.

As shown in Figure 3a−d, the morphology of thin films of **1** undergoes apparent change with increasing substrate temperatures (T_{sub}). When evaporated at rt, rodlike grains with certain terrace structures (Figure S13a) are observed. With T_{sub} increasing, the grains continuously grow larger in size. However, the grain boundaries simultaneously become much more obvious and grow deeper in depth at T_{sub} = 120 °C, which shows negative influence on the charge-transport performance. The corresponding XRD patterns at rt appear amorphous-like without any detectable diffraction peaks (Figure S14). With T_{sub} increasing, from rt to 80 °C, and further to 120 °C, the films clearly show a first-order diffraction peak with relatively high intensity. In addition, multi-order diffraction peaks appear at larger 2-θ values. The results suggest high degrees of crystallinity and molecular ordering are formed

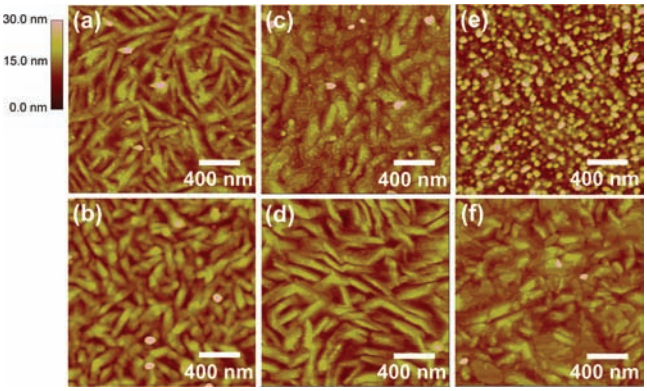

Figure 3. AFM images of vapor-deposited films based on **1** on OTS-modified Si/SiO_2 substrate at (a) room temperature; (b) 80 °C; (c,e) 100 °C; (d,f) 120 °C. Films of (a−d) are deposited with a normal rate, and (e−f), with a much faster rate.

in the thin films. However, at T_{sub} = 120 °C, the grain boundaries become larger and deeper as mentioned above (Figure 3d), which might be unfavorable for charge transport. Regardless of the variation of the T_{sub}, the first-order diffraction peak always appears at 5.5° with a *d*-spacing of ∼16.2 Å, corresponding to the thickness of a molecular monolayer. The molecular orientation on the substrate can be estimated by comparing the monolayer thickness with the actual molecular length. On the basis of the aforementioned single-crystal data, molecular length might be 15.024, 16.228, and 16.600 Å along the shorter (ethyl), longer (hexyl) branched alkyl chain, and π-conjugated aromatic quinoidal core directions, respectively (Figure S15). In comparison with the *d*-spacing (16.2 Å), the molecular lengths along distinct directions are nearly of the same order, indicating the equal possibility for molecular packing along each direction. However, considering the similarity and compatibility of alkyl groups with OTS-modified SiO_2/Si substrate opposed to those with aromatic π-conjugated backbone, we believe that the molecules are more inclined to exhibit end-to-end packing conformation on the substrate along the alkyl (ethyl or hexyl) directions in thin films. Additionally, the effect of the vapor evaporation rate on the thin film properties was also studied for several T_{sub}'s (100, 120, and 150 °C; see Figures S16−S18), which is expected to optimize the film properties and in turn further improve the electron-transport performance for **1**. AFM images (Figure 3e,f) reveal that the morphologies can be greatly modified when the deposition rate is adjusted while maintaining T_{sub} at the same value. Notably, granular grains with well-formed terrace structures (Figure S13b) are formed at 120 °C with an adjusted deposition rate, manifesting high film quality with much better uniformity and continuity compared to thin films deposited with a normal rate at the same T_{sub}. The corresponding XRD patterns (Figures S16 and S17) show mainly two features; one is the great increase in the intensity of peaks, especially for the first-order diffraction peak, along with a much sharper shape; the other is the appearance of multi-order diffraction peaks up to fifth order, both of which reveal extensively improved crystallinity[20] and a higher degree of molecular ordering in the thin films when deposited with an adjusted rate, both of which are favorable for improving charge-transport performance.

For **2**, the morphology and ordering of the spin-coated thin films were studied as a function of thermal annealing temperature. As shown in the AFM images (Figure S19), the as-spun film exhibits a fibrillar network of granular features with good uniformity and continuity. After a thermal annealing treatment, the grains grow slightly larger in size. However, XRD patterns show evident variation at different annealing temperatures (Figure S20). The intensity of the peaks continuously increases to a maximum value after annealing at 120 °C, and multi-order peaks could be observed, which further demonstrates the high crystallinity of thin film. The first-order diffraction peak of a thin film based on **2** appears at much smaller 2-θ angles (3.6°) with a *d*-spacing of ∼24.0 Å, which is larger than that of **1**. Considering that the molecular length along the long π-conjugated molecular axis should be the same, this increase might be ascribed to the expansion of the alkyl groups perpendicular to the long molecular axis of the π-conjugated skeleton. In order to further understand the molecular orientation on the substrate, theoretical calculation was carried out to simulate the molecular length. According to the theoretical result, the molecular lengths of **2** along both

dx.doi.org/10.1021/ja3003183 | J. Am. Chem. Soc. 2012, 134, 4084−4087

branched alkyl directions are the same, ~25.0 Å (Figure S21), which is well in agreement with the monolayer thickness. Therefore, we speculate that the molecules tend to present end-to-end molecular packing configuration on the OTS-modified SiO_2/Si substrate along the alkyl (hexyl or decyl) stretching direction in thin films, which is similar to that for **1**.

In addition, note that the electron mobility of both **1** and **2** could reach the order of more than 0.1 $cm^2 V^{-1} s^{-1}$ when films based on **1** and **2** are vapor-deposited and as-spun at rt, respectively. This result is somewhat surprising because films based on **1** and **2** when "as deposited or spun" appear to be amorphous-like (Figures S14 and S20). Therefore, we speculate the relatively high performance might be the result of either the smooth and uniform thin film morphology or the strong intermolecular interactions deduced from the UV−vis spectra of the thin films, both of which are of great advantage for charge transport. In fact, such a high performance based on amorphous-like thin films is rarely observed for small molecules,[21] for which a postdeposition thermal treatment step is generally required to obtain optimal device characteristics. Meanwhile, the maximum electron mobilities based on **1** and **2** have achieved several times or 1 order of magnitude improvement when compared to those of other oligomer-based quinoidal materials, including oligothiophene and selenophene/pyrrole-containing derivatives. Moreover, the devices based on **1** showed good air stability over a period of about two weeks, with a nearly identical electron mobility of 0.48 $cm^2 V^{-1} s^{-1}$ and stable I_{on}/I_{off} of 10^6 (Figure S22). The **1**-based OFETs also exhibited satisfactory operating stability during the cycle test (5000 times, Figure S23).

In summary, we have developed a novel series of DPP-containing quinoidal small molecules as n-type OSCs for application in OFETs. The representatives of this species **1** and **2** with branched alkyl substituent have been successfully applied as active semiconducting layers for high-performance, ambient-stable, and even solution-processable n-channel OFETs. Under ambient conditions, the maximum electron mobility on vapor-processed films was up to 0.55 $cm^2 V^{-1} s^{-1}$ with I_{on}/I_{off} of 10^6, whereas electron mobility for solution-processed films was 0.35 $cm^2 V^{-1} s^{-1}$ with I_{on}/I_{off} of 10^5−10^6. The results demonstrate that these DPP-based quinoidal small molecules, especially ones with longer branched alkyl groups, are promising candidates for low-cost, large-area organic electronics.

■ ASSOCIATED CONTENT

Supporting Information

Details of synthesis and characterization of **1** and **2** and details of OTFT device fabrication and characterization. This material is available free of charge via the Internet at http://pubs.acs.org.

■ AUTHOR INFORMATION

Corresponding Author

wxu@iccas.ac.cn; liuyq@iccas.ac.cn; zhudb@iccas.ac.cn

Notes

The authors declare no competing financial interest.

■ ACKNOWLEDGMENTS

Financial support from the National Natural Science Foundation of China (61101051, 20952001, 21021091), the State Key Basic Research Program (2011CB808401), and the Chinese Academy of Sciences is acknowledged.

■ REFERENCES

(1) (a) Dimitrakopoulos, C. D.; Malenfant, P. R. L. *Adv. Mater.* **2002**, *14*, 99. (b) Sun, Y. M.; Liu, Y. Q.; Zhu, D. B. *J. Mater. Chem.* **2005**, *15*, 53. (c) Mas-Torrent, M.; Rovira, C. *Chem. Soc. Rev.* **2008**, *37*, 827.

(2) Voss, D. *Nature* **2000**, *407*, 442.

(3) (a) Andersson, P.; Forchheimer, R.; Tehrani, P.; Berggren, M. *Adv. Funct. Mater.* **2007**, *17*, 3074. (b) Huitema, H. E. A.; Gelinck, G. H.; van der Putten, J. B. P. H; Kuijk, K. E.; Hart, C. M.; Cantatore, E.; Herwig, P. T.; van Breemen, A. J. J. M.; de Leeuw, D. M. *Nature* **2001**, *414*, 599.

(4) (a) Crone, B. K.; Dodabalapur, A.; Sarpeshkar, R.; Gelperin, A.; Katz, H. E.; Bao, Z. *J. Appl. Phys.* **2002**, *91*, 10140. (b) Lin, Y.-Y.; Dodabalapur, A.; Sarpeshkar, R.; Bao, Z.; Li, W.; Baldwin, K.; Raju, V. R.; Katz, H. E. *Appl. Phys. Lett.* **1999**, *74*, 2714.

(5) (a) Newman, C. R.; Frisbie, C. D.; da Silva Filho, D. A.; Brédas, J.-L.; Ewbank, P. C.; Mann, K. R. *Chem. Mater.* **2004**, *16*, 4436. (b) Wen, Y. G; Liu, Y. Q. *Adv. Mater.* **2010**, *22*, 1331.

(6) Guo, X. G.; Ortiz, R. P.; Zheng, Y.; Hu, Y.; Noh, Y.-Y.; Baeg, K.-J.; Facchetti, A.; Marks, T. J. *J. Am. Chem. Soc.* **2011**, *133*, 1405.

(7) (a) Usta, H.; Facchetti, A.; Marks, T. J. *J. Am. Chem. Soc.* **2008**, *130*, 8580. (b) Yan, H.; Chen, Z. H.; Zheng, Y.; Newman, C.; Quinn, J. R.; Dötz, F.; Kastler, M.; Facchetti, A. *Nature* **2009**, *457*, 679.

(8) Wu, Q. H.; Li, R. J.; Hong, W.; Li, H. X.; Gao, X. K.; Zhu, D. B. *Chem. Mater.* **2011**, *23*, 3138.

(9) Pappenfus, T. M.; Chesterfield, R. J.; Frisbie, C. D.; Mann, K. R.; Casado, J.; Raff, J. D.; Miller, L. L. *J. Am. Chem. Soc.* **2002**, *124*, 4184.

(10) Handa, S.; Miyazaki, E.; Takimiya, K.; Kunugi, Y. *J. Am. Chem. Soc.* **2007**, *129*, 11684.

(11) (a) Suzuki, Y.; Miyazaki, E.; Takimiya, K. *J. Am. Chem. Soc.* **2010**, *132*, 10453. (b) Suzuki, Y.; Shimawaki, M.; Miyazaki, E.; Osaka, I.; Takimiya, K. *Chem. Mater.* **2011**, *23*, 795.

(12) (a) Nelson, T. L.; Young, T. M.; Liu, J. Y.; Mishra, S. P.; Belot, J. A.; Balliet, C. L.; Javier, A. E.; Kowalewski, T.; McCullough, R. D. *Adv. Mater.* **2010**, *22*, 4617. (b) Li, Y. N.; Singh, S. P.; Sonar, P. *Adv. Mater.* **2010**, *22*, 4862. (c) Cho, S.; Lee, J.; Tong, M. H.; Seo, J. H.; Yang, C. *Adv. Funct. Mater.* **2011**, *21*, 1910.

(13) (a) Loser, S.; Bruns, C. J.; Miyauchi, H.; Ortiz, R. P.; Facchetti, A.; Stupp, S. I.; Marks, T. J. *J. Am. Chem. Soc.* **2011**, *133*, 8142. (b) Wienk, M. M.; Turbiez, M.; Gilot, J.; Janssen, R. A. J. *Adv. Mater.* **2008**, *20*, 2556.

(14) (a) Cao, D. R.; Liu, Q. L.; Zeng, W. J.; Han, S. H.; Peng, J. B.; Liu, S. P. *Macromolecules* **2006**, *39*, 8347. (b) Beyerlein, T.; Tieke, B.; Forero-Lenger, S.; Brütting, W. *Synth. Met.* **2002**, *130*, 115.

(15) (a) Mohebbi, A. R.; Yuen, J.; Fan, J.; Munoz, C.; Wang, M. F.; Shirazi, R. S.; Seifter, J.; Wudl, F. *Adv. Mater.* **2011**, *23*, 4644. (b) Bronstein, H.; Chen, Z. Y.; Ashraf, R. S.; Zhang, W. M.; Du, J. P.; Durrant, J. R.; Tuladhar, P. S.; Song, K.; Watkins, S. E.; Geerts, Y.; Wienk, M. M.; Janssen, R. A. J.; Anthopoulos, T.; Sirringhaus, H.; Heeney, M.; McCulloch, I. *J. Am. Chem. Soc.* **2011**, *133*, 3272.

(16) (a) Tantiwiwat, M.; Tamayo, A.; Luu, N.; Dang, X.-D.; Nguyen, T.-Q. *J. Phys. Chem. C* **2008**, *112*, 17402. (b) Zhang, Y.; Kim, C.; Lin, J.; Nguyen, T.-Q. *Adv. Funct. Mater.* **2012**, *22*, 97.

(17) Uno, M.; Seto, K.; Takahashi, S. *J. Chem. Soc. Chem. Comm.* **1984**, 932.

(18) (a) Anthopoulos, T. D.; Anyfantis, G. C.; Papavassiliou, G. C.; de Leeuw, D. M. *Appl. Phys. Lett.* **2007**, *90*, 122105. (b) Usta, H.; Risko, C.; Wang, Z. M.; Huang, H.; Deliomeroglu, M. K.; Zhukhovitskiy, A.; Facchetti, A.; Marks, T. J. *J. Am. Chem. Soc.* **2009**, *131*, 5586.

(19) (a) Guo, X. G.; Ortiz, R. P.; Zheng, Y.; Kim, M.-G.; Zhang, S. M.; Hu, Y.; Lu, G.; Facchetti, A.; Marks, T. J. *J. Am. Chem. Soc.* **2011**, *133*, 13685. (b) Bouchard, J.; Belletête, M.; Durocher, G.; Leclerc, M. *Macromolecules* **2003**, *36*, 4624.

(20) (a) Lee, H. S.; Kim, D. H.; Cho, J. H.; Park, Y. D.; Kim, J. S.; Cho, K. *Adv. Funct. Mater.* **2006**, *16*, 1859. (b) Meng, Q.; Jiang, L.; Wei, Z. M.; Wang, C. L.; Zhao, H. P.; Li, H. X.; Xu, W.; Hu, W. P. J *Mater. Chem.* **2010**, *20*, 10931.

(21) Beaujuge, P. M.; Fréchet, J. M. J. *J. Am. Chem. Soc.* **2011**, *133*, 20009.